Biophysical Chemistry 139 (2009) 75–83

Contents lists available at ScienceDirect

Biophysical Chemistry

journal homepage: http://www.elsevier.com/locate/biophyschem

# Dibucaine effects on structural and elastic properties of lipid bilayers

G.S. Lorite [a,*], T.M. Nobre [b,1], M.E.D. Zaniquelli [b], E. de Paula [c], M.A. Cotta [a]

[a] Universidade Estadual de Campinas, Instituto de Física Gleb Wataghin, Departamento de Física Aplicada, Campinas, SP, Brazil
[b] Universidade de São Paulo — Faculdade de Filosofia Ciências e Letras de Ribeirão Preto, Departamento de Química, Ribeirão Preto, SP, Brazil
[c] Universidade Estadual de Campinas, Instituto de Biologia, Departamento de Bioquímica, Campinas, SP, Brazil

ARTICLE INFO

*Article history:*
Received 15 July 2008
Received in revised form 17 October 2008
Accepted 20 October 2008
Available online 31 October 2008

*Keywords:*
Lipid bilayers
Local anesthetic
Dibucaine
AFM
Dynamic surface tension
Dilatational surface elasticity

ABSTRACT

In this work we report the interaction effects of the local anesthetic dibucaine (DBC) with lipid patches in model membranes by Atomic Force Microscopy (AFM). Supported lipid bilayers (egg phosphatidylcholine, EPC and dimyristoylphosphatidylcholine, DMPC) were prepared by fusion of unilamellar vesicles on mica and imaged in aqueous media. The AFM images show irregularly distributed and sized EPC patches on mica. On the other hand DMPC formation presents extensive bilayer regions on top of which multibilayer patches are formed. In the presence of DBC we observed a progressive disruption of these patches, but for DMPC bilayers this process occurred more slowly than for EPC. In both cases, phase images show the formation of small structures on the bilayer surface suggesting an effect on the elastic properties of the bilayers when DBC is present. Dynamic surface tension and dilatational surface elasticity measurements of EPC and DMPC monolayers in the presence of DBC by the pendant drop technique were also performed, in order to elucidate these results. The curve of lipid monolayer elasticity versus DBC concentration, for both EPC and DMPC cases, shows a maximum for the surface elasticity modulus at the same concentration where we observed the disruption of the bilayer by AFM. Our results suggest that changes in the local curvature of the bilayer induced by DBC could explain the anesthetic action in membranes.



## 1. Introduction

Supported lipid bilayers (SLBs) have been widely employed as model systems both for the elucidation of basic processes occurring in biological membranes as well as for some biotechnological applications [1–8]. The potential of supported lipid bilayers in this area has attracted great interest in the last few years since drug interaction with model membranes can be used to assess its biological activity [9].

Supported planar bilayers can be formed by the adsorption of phospholipids on a planar solid support. In pharmaceutical research, liposomes have been used as drug-delivery systems and as models for studying drug membrane interactions [9]. A variety of methods has been used on artificial membranes. The results have demonstrated that the membrane properties may be strongly affected by the presence of membrane-associated molecules. The conformation of acyl groups, the membrane surface and thickness as well as membrane fusion properties are examples of parameters than can be affected by drug–membrane interactions [10–12]. In particular, among these drugs, local anesthetic reversibly inhibits the propagation of electric impulses along nerves. The literature shows many theories about the mechanism of action of local anesthetics [13–16]. Most of them are focused on the direct effect of local anesthetics on the sodium channel protein — thus inhibiting the propagation of the action potential responsible for the nervous impulse, while others consider the interaction of anesthetic molecules with the lipid phase of the membrane. This particular interaction could induce changes in the membrane lipids properties such as mobility or conformation, and affect the sodium channel insertion in the bilayer, making it inactive and causing anesthesia [17,18].

The interest in SLB systems arose after the development of analytica – microscopic or spectroscopic – techniques applied to interfaces [19,20]. These techniques have contributed to our understanding of some membrane properties, like rafts and lipid domains present in this structure [21,22]. Among these techniques, AFM has been used to monitor time dependent processes such as insertion of proteins into model cells [23,24] and the growth of single lipid domains in lipid bilayers. In addition, it is possible to follow the evolution of the interaction of drugs, peptides or other molecules of interest with Langmuir monolayers (considered as a biomembrane model) through surface tension curves and several dynamic measurements [25,26].

In this study, we present the real-time observation of the interaction between the local anesthetic dibucaine (DBC) and lipid patches in model membranes by Atomic Force Microscopy (AFM). We have also used adsorption kinetics and dilatational surface elasticity measurements to analyze dibucaine-membrane interaction. Supported egg phosphatidylcholine (EPC) and dimyristoylphosphatidyl-

* Corresponding author. UNICAMP – IFGW – DFA, CP 6165 – Cidade Universitária Zeferino Vaz, 13083-970 – Campinas, SP, Brazil. Tel.: +55 19 35215360.
*E-mail address:* glorite@ifi.unicamp.br (G.S. Lorite).
[1] Present Address: Universidade de São Paulo- Instituto de Física de São Carlos, São Carlos, SP, Brazil.

0301-4622/$ – see front matter © 2008 Elsevier B.V. All rights reserved.
doi:10.1016/j.bpc.2008.10.006

choline (DMPC) were formed on mica using the vesicle fusion method [28,29]. Topography and phase images were acquired on the lipid membrane in the absence or presence of DBC. Local changes in curvature were observed depending on concentration range of DBC, leading to an eventual disruption of the bilayer. AFM results, obtained from bilayers samples, were correlated to dynamic elasticity measurements performed with monolayers. The results presented in this work support local curvature models for the transport of molecules across biomembranes.

## 2. Materials and methods

### 2.1. Materials

L-α-phosphatidylcholine (EPC) and 1,2 dimyristoyl-phosphatidilcholine (DMPC) (Avanti Polar-Lipids INC., Albaster, AL, USA) were used without further purification. Deionized, nanopure quality water was used for the preparation of vesicles. Freshly cleaved muscovite mica (TED Pella Inc., USA) was used as a substrate for AFM measurements. Dibucaine hydrochloride (Sigma Aldrich Co., St. Louis, MO, USA) was dissolved in deionized water (protonated form) and thereafter diluted to the desired concentrations.

### 2.2. Preparation of lipid bilayers

Supported planar bilayers were prepared for AFM imaging by the method of vesicle fusion [28,29] as follows. Phospholipid was dissolved in chloroform and dried using a stream of dry nitrogen to remove possible traces of the solvent. The lipid was then re-suspended from the walls of the eppendorf tube by vigorous vortexing in water. To obtain small unilamellar EPC vesicles (SUVs), the suspension went through an average of 15 intermittent cycles of sonication (30 s of ultrasound – 20 kHz frequency – followed by 30 s pause) in a Sonics & Materials Inc, VC50. The suspension was kept in an ice bath to avoid superheating during the whole process. SUV suspension was then diluted to 0.1 mM. For the DMPC case, SUVs were obtained by extrusion (12 times) through a pair of 0.1 μm polycarbonate filters (Poretics). In this case, the SUV suspension was diluted to 2 mM. In both cases, different volumes of the SUV suspension were put into contact with unmodified freshly cleaved mica. After a controlled period of time (incubation time) the mica surfaces were observed by Atomic Force Microscopy at room temperature (25 °C).

### 2.3. AFM imaging

AFM images were acquired with an Agilent 5500 equipment, using MAC (magnetic A/C) mode, where a magnetically-coated probe oscillates near its resonant frequency driven by an alternating magnetic field. The nominal spring constant of the Type I MAClevers used here was 1.75 N/m; the radius of curvature of these tips was estimated to be <10 nm. All imaging was performed in a liquid cell with deionized water.

DBC was incorporated to the solution by adding small volumes of anesthetic into the liquid cell, containing the supported bilayer on mica. Topography images of the bilayer without DBC were acquired for at least an hour, in order to determine membrane stability under the chosen scanning conditions. Subsequently, DBC solution was added into the AFM liquid cell in single or several steps, according to the desired experiment. The minimum DBC solution volume for each step was 0.02 ml; we stopped DBC addition when the maximum volume of the liquid cell (0.6 ml) was reached. The experiments on EPC and DMPC intended to observe bilayer changes with increasing DBC concentration, initially from 0 to 8 mM and later in a narrower range (according to the effects observed). The DBC concentrations mentioned hereafter are the final values in the liquid cell (considering initial water plus added DBC volume).

### 2.4. Langmuir monolayers

The surface pressure-area curves for EPC and DMPC were obtained by spreading chloroform solutions of each phospholipid in a Langmuir trough (Insight, Brazil) and upon compressing the monolayers at a surface rate of 2.4 $Å^2$ $molecule^{-1}$ $s^{-1}$, after waiting for solvent evaporation for ca. 15 min, at 24 °C.

### 2.5. Adsorption Kinetics at air/liquid interface

The adsorption of dibucaine at lipid monolayers was carried out by surface tension measurements, by the pendant drop method with axisymmetric drop shape analysis, using an automatic contact-angle-tensiometer OCA-20, from Dataphysics, Germany, as described previously [27]. For the experiments, a small drop of the dibucaine solution in concentration below its critical micelle concentration (CMC) was formed and a solution of the lipid was suitably touched on the surface of the drop, in order to form a Langmuir monolayer. After that, the drop was expanded up to the surface pressure of 30 mN $m^{-1}$ which corresponds to the lipid packing of a biomembrane [30]. Then, the surface tension values were followed until the system reached the equilibrium, considered as a variation <0.5 mN $m^{-1}$, in 60 s.

### 2.6. Dilatational elasticity

For dilatational surface elasticity measurements the same apparatus was used, with the addition of a frequency oscillator that promotes sinusoidal disturbance in the drop, resulting in different area values [31,32]. The dilatational surface elasticity ($\varepsilon$) or surface elasticity modulus is related with the ability of the system to establish a new surface tension value after an area change, and its equilibrium value ($\boldsymbol{E}$) is defined according to Gibbs:

$$\boldsymbol{E} = d\gamma / d\ln A. \quad (1)$$

where $\gamma$ and $A$ are the surface tension and area, respectively. Under dynamic conditions, films range from perfectly viscous to perfectly elastic, with the latter occurring only when no relaxation process takes place. This is detected experimentally by a zero phase difference given by the phase angle, $\varphi$, between the perturbation (deformation) and the response of the system (change in surface tension). On the other hand, phase differences are characteristic of an interfacial viscoelastic behavior. This feature is accounted for introducing the complex modulus:

$$\boldsymbol{E} = |\varepsilon|\cos\varphi + \boldsymbol{i}|\varepsilon|\sin\varphi. \quad (2)$$

The imaginary part of this quantity accounts for the energy dissipation process which may involve loss of the monolayer arrangement, and is related to surface dilatational viscosity. The drop oscillation was initiated after the surface tension of the system reached a constant value. The frequency applied was 1.2 Hz, with a relative deformation of 5.5%. All experiments at air/liquid interface were carried out at 25±1 °C.

## 3. Results and discussion

### 3.1. EPC and DMPC bilayer patches

Topographic images of the supported EPC bilayers are shown in Fig. 1 (A, B). These images revealed different formation of EPC planar bilayers and can be attributed to the volume of SUV suspension and the incubation time used in the preparation of the supported bilayer [29,33,34]. Fig. 1A illustrate a typical EPC patch on mica obtained after addition of 2 μl SUV suspension on mica, with 2 h of incubation. The thickness of the EPC patch observed was 5.5±0.3 nm (average of 100 cross section measurements). However, by increasing the volume (60 μl) and the incubation time (3 h) we could observe multi-bilayer

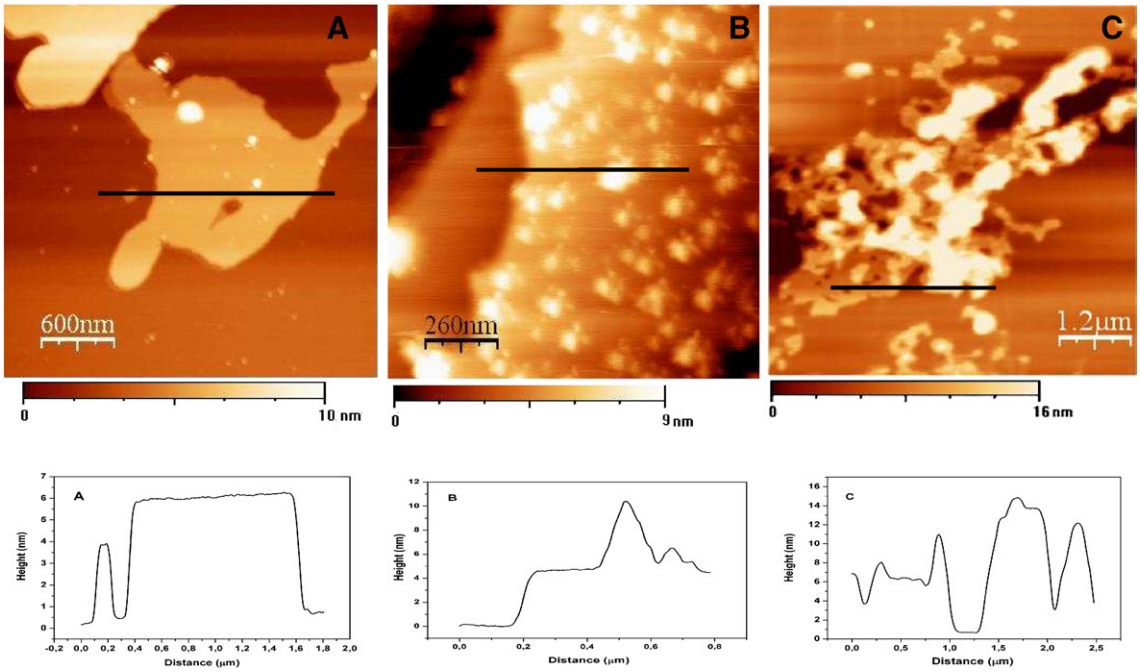


**Fig. 1.** Typical topographic images with respective cross sections of: (A) EPC patches on mica (2 μl SUV suspension in water (0.1 mM) on mica with 2 h of incubation), (B) EPC multi-bilayer with EPC aggregates (60 μl SUV suspension in water (0.1 mM) on mica with 3 h of incubation) and (C) DMPC patches on the DMPC bilayer surface (10 μl SUV suspension in water (2 mM) on mica with 2 h of incubation).

formation with EPC aggregation on the surface (Fig. 1B). Yuan and Johnston [33] have studied the conditions for obtaining a uniform EPC planar bilayer on mica. In agreement with our experiments, they observed EPC patches formed after 15 min. of incubation and complete EPC bilayer, after 45 min. Reviakine and Brisson [34] described several features of the process of supported bilayer formation from SUVs on mica, including EPC bilayer formation. They showed that the adsorption of intact vesicles preceded the formation of bilayer patches. Egawa and Furusawa [29] observed EPC vesicles adsorbed on mica after short incubation times (5 min) and EPC patches with increasing incubation times, up to 4 h, when a complete EPC bilayer was formed on mica. Therefore, even though our incubation times were longer, the observed trend in our results for EPC bilayer formation are consistent with the literature.

Previous works [35–38] revealed that the interaction between DBC and PC phospholipids occurs at the bilayer surface. Thus we have also prepared DMPC bilayers since they are usually more ordered and compact than EPC bilayers, while keeping the same polar head group. Our experiments show the formation of extensive DMPC bilayers with DMPC patches on the surface (suggesting the formation of a new, incomplete, DMPC bilayer), as shown by the topographic image in Fig. 1C. Indentations carried out on these samples with the AFM tip have actually shown that multi-bilayers (at least 6–7 bilayers high) are formed on the mica (see supplementary information). The thickness of the DMPC patches on the extensive DPMC multi-bilayer surface was measured as 5.0±0.6 nm (average of 50 cross section measurements). These results could be compared to the literature; Dvorak et al [39] have also observed extensive DMPC multi-bilayer formation which they attributed to the long incubation time. It is important to notice that our experiments were carried out above the gel to fluid phase transition temperature of DMPC (24 °C, according to Granick et al. [40]).

For both DMPC and EPC bilayers, we have chosen to investigate the DBC interaction with use of multi-bilayer surfaces. Due to the electrostatic interaction, different elastic behaviors could be expected for the bilayer patches formed directly on mica, as compared to those on top of the multi-bilayers — the latter more closely resembling a biological system. Moreover, since in our experiments DBC is protonated, the presence of the multi-bilayer would also screen any possible DBC interactions with the mica surface as well.

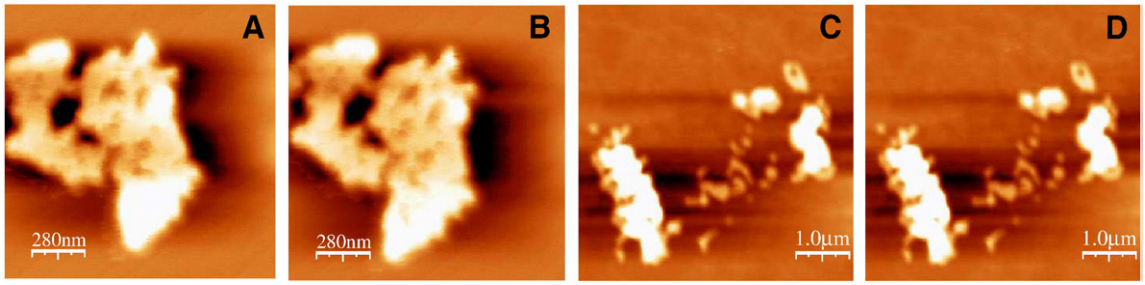


**Fig. 2.** Topographic images of EPC (A, B; z-scale: 8 nm) and DMPC (C, D; z-scale: 12 nm) supported bilayers on mica to assess the stability of domains. (A) EPC patch (2 μl SUV suspension in water (0.1 mM) on mica with 2 h of incubation) — first image. (B) the same EPC patch in image (A) after scanning the surface for 140 min. (C) DMPC patch (10 μl SUV suspension in water (2 mM) on mica with 2 h of incubation) — first image. (D) the same DMPC patch in image (C) after scanning the surface for 90 min.

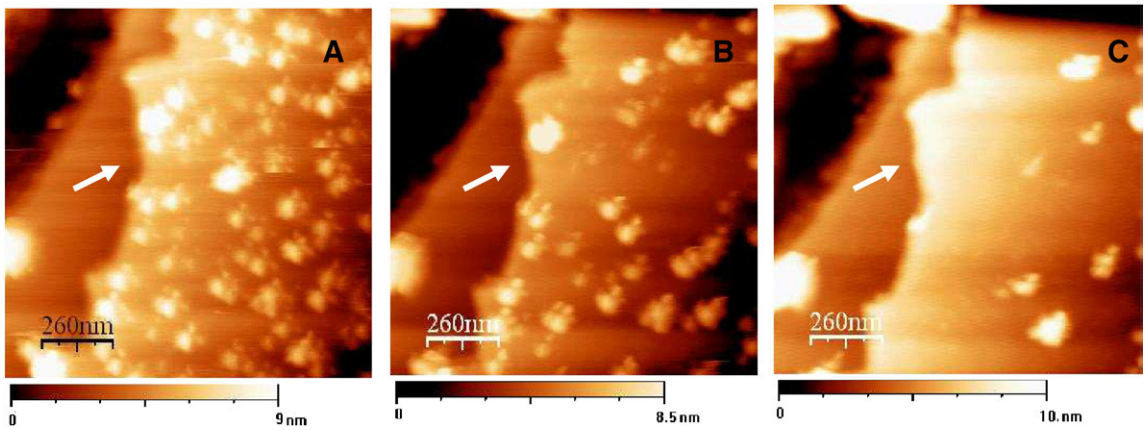


**Fig. 3.** Topographic images of EPC multi-bilayer with EPC aggregates on the surface (60 μl SUV suspension in water (0.1 mM) on mica with 3 h of incubation) acquired with increasing DBC concentration in the liquid cell. (A) No DBC in the liquid cell. (B) After 2nd addition of DBC (final concentration in the liquid cell: 2.72 mM). (C) After 8th addition of DBC (final concentration in the liquid cell: 6.30 mM). DBC effect: progressive disappearance of the EPC aggregates. A double tip artifact can be observed in the figures but it does not affect the qualitative behavior reported here.

To assess the stability of EPC and DMPC bilayers during consecutive scanning in aqueous media, successive images of the same bilayer region were acquired. As shown in Fig. 2, scanning the lipid patches for a few hours did not cause any significant change in the bilayer overall morphology, indicating that bilayers were stable under these conditions.

### 3.2. Interaction between DBC and supported lipid bilayers

Topographic images of supported EPC and DMPC bilayers were acquired at the same region before and after DBC addition. In the EPC case, we observed a few morphological changes with increasing DBC concentration. A selection of topographic images with 0 mM, 2.72 mM and 6.30 mM of DBC is shown in Fig. 3. After the first addition (image not shown), the EPC morphology was similar to that obtained in the absence of DBC. However, after the second addition (2.72 mM) we observed a progressive disappearance of the EPC aggregates on the bilayer surface with increasing DBC concentration in the liquid cell (Fig. 3 B and C). However, although the aggregates vanished in the images, we could not observe significant changes at the EPC bilayer edges (arrows, Fig. 3), indicating that they were still stable under these conditions. For DMPC bilayers, Fig. 4 shows the time evolution of morphological changes with a single DBC addition (5 mM concentration). About 1 h after DBC addition we could observe the rupture of small DMPC patches (Fig. 4B — arrows). Increasing the DBC incubation time led to a progressive disruption of the bilayer patch, eventually washing out any step feature representative of a bilayer image. Fig. 5 shows a sequence of cross sections for different times after DBC addition into liquid cell with DMPC bilayer patch. We can observe from this figure that the patches gradually shrink in size; rupture occurs after ca. 1.5 h from the beginning of the experiment. These results could also be attributed to variation of the partition coefficient (P) with DBC concentration [42]. However, based on previous works reported in literature [36,41] we believe this is not the case. Furthermore, a possible variation of P does not invalidate our AFM data since, for both experiments reported here (one of them where DBC concentration is kept constant), morphology changes follow the same trend.

Fig. 6 shows the phase image of the EPC and DMPC bilayers before and after DBC addition, acquired simultaneously with the scans shown in Figs. 3 and 4. In both cases, we can observe a different contrast over the bilayer surface after DBC addition (Fig. 6 B, C, E and F). The contrast in the phase images is often interpreted as differences in surface viscoelasticity or tip-surface energy dissipation [28]. The stability in the simultaneously acquired topography images indicates that the variations in phase images are not tip-related (for example, due to DBC

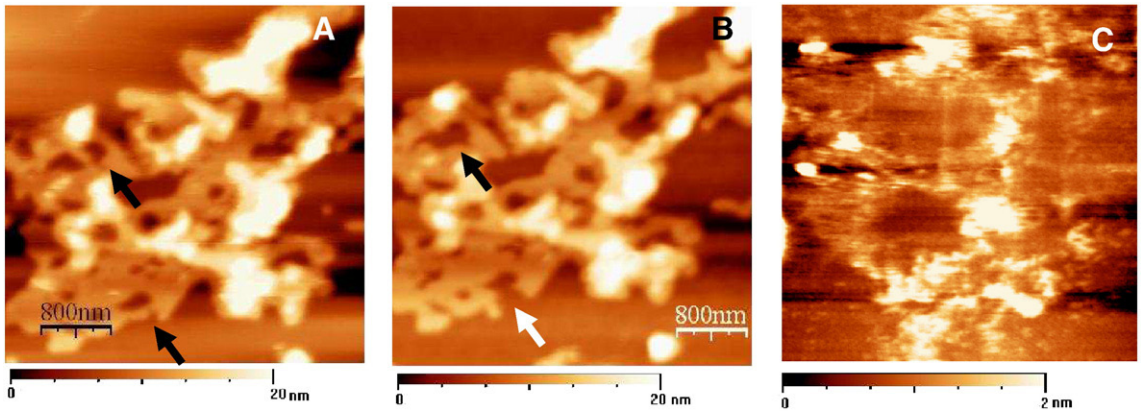


**Fig. 4.** Topographic images of DMPC patch (10 μl SUV suspension in water (2 mM) on mica with 2 h of incubation) acquired along the time after a single DBC addition into the liquid cell(final concentration in the liquid cell: 5 mM). (A) No DBC in the liquid cell. (B) After 1 h of DBC addition. (C) After 2 h 30 min DBC addition. DBC effect: progressive disruption (arrows) and disappearance of the bilayer patch.

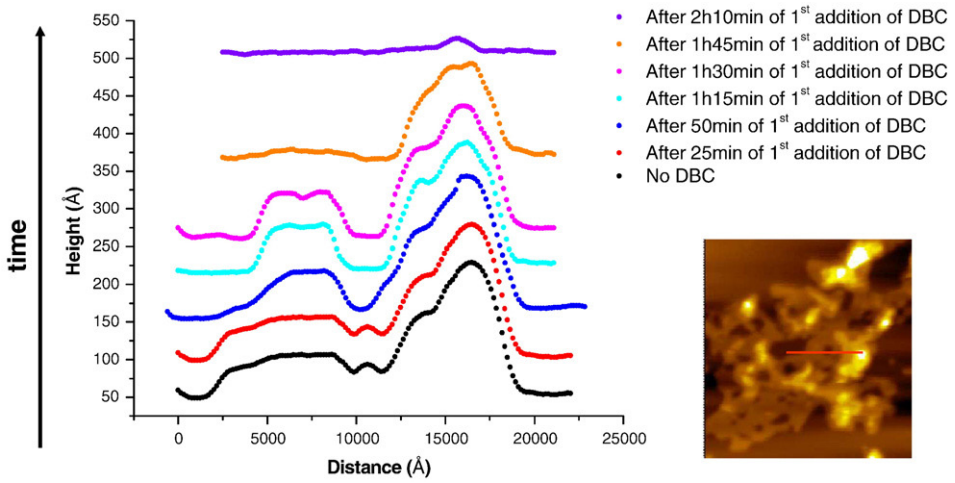


**Fig. 5.** Time evolution sequence of cross sections of a DMPC patch on the extensive DMPC bilayer surface (10 μl SUV suspension in water (2 mM) on mica with 2 h of incubation) without DBC and after DBC addition into liquid cell (final concentration in the liquid cell: 5 mM). Right: topography image of DMPC patch without DBC showing the position where the cross section was acquired.

interaction with the tip). In this particular case, we believe that DBC changes the viscoelastic properties of the lipid bilayer. To test this hypothesis, experiments on viscoelastic properties of phospholipid layers have also been performed at the liquid–air interface, and are presented in Section 3.4.

In association with the contrast observed in the phase images, height variations (0.05–0.2 nm) throughout all multibilayer surfaces show up in the topography images — newly "budding" structures. Fig. 7 shows topographic images for the regions where contrast is observed in the phase image. Amino local anesthetics such as dibucaine can form micelles in solution when the concentration exceeds the CMC [37]. In addition, the literature suggests that DBC binds to polar head group of EPC, i.e., that DBC is inserted mainly on the bilayer surface [35–38], eventually as a dimer [37,43]. In fact, Ueda et al [38] suggested that dibucaine destabilize lipid bilayers by competing for the phosphate group and breaking previously existing

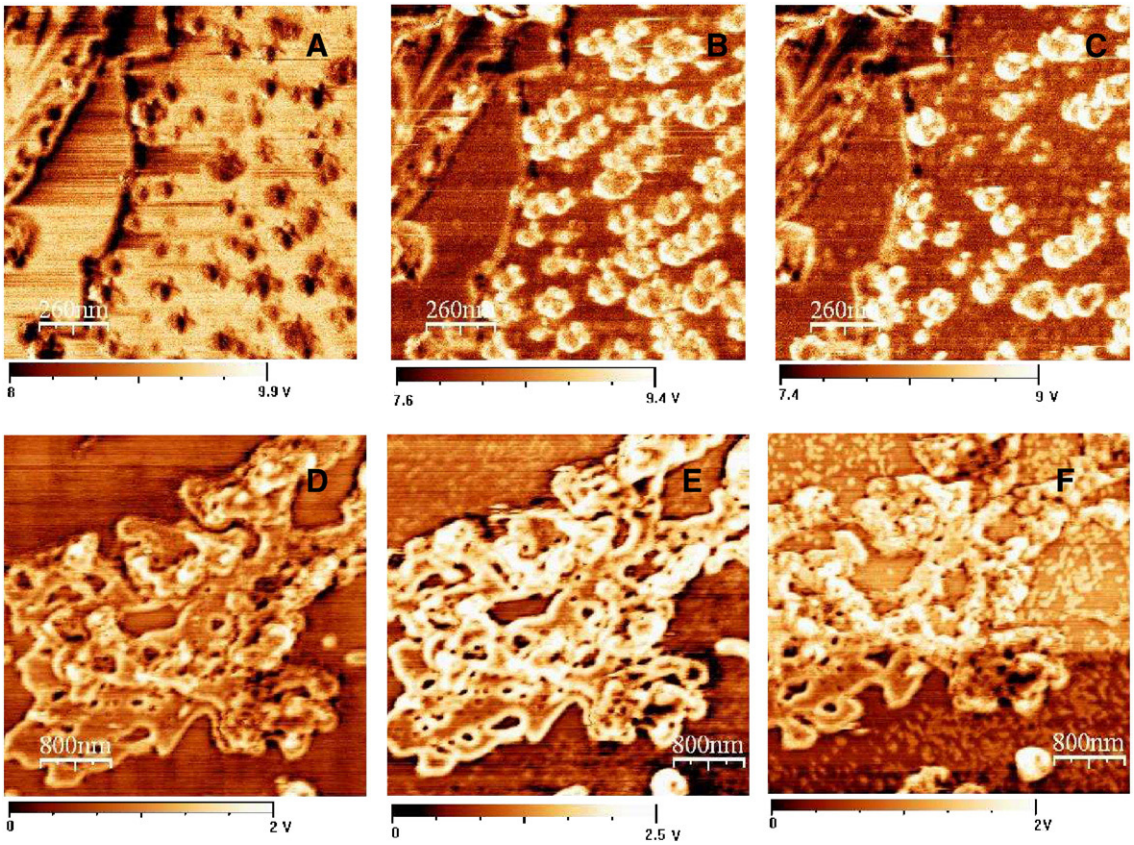


**Fig. 6.** Phase images of EPC (A, B, C — 60 μl SUV suspension in water (0.1 mM) on mica with 3 h of incubation) and DMPC (D, E, F — 10 μl SUV suspension in water (2 mM) on mica with 2 h of incubation) supported bilayers, showing a progressive contrast formation on the surfaces. (A) EPC without DBC in liquid cell. (B) EPC after 2nd addition of DBC (final concentration in liquid cell: 2.72 mM). (C) EPC after 8th addition of DBC (final concentration in liquid cell: 6.30 mM). (D) DMPC without DBC in liquid cell. (E) DMPC after 1 h of single DBC addition (final concentration in the liquid cell: 5 mM). (F) DMPC after 2 h 30 min of single DBC addition (final concentration in the liquid cell: 5 mM).

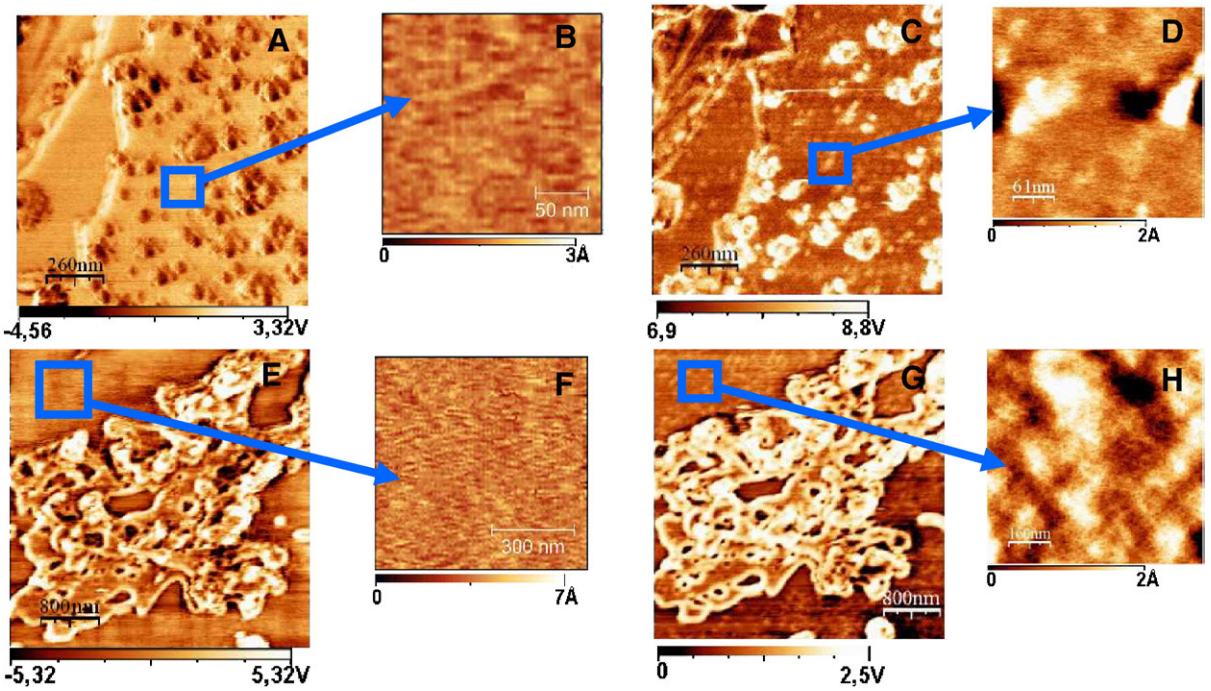


**Fig. 7.** (A) Phase image of EPC multi-bilayer with EPC aggregates on the surface. Blue square: region of the EPC bilayer surface where a small area topographic image (B) was acquired. (C) Phase image of the same structures in (A) after DBC addition. Blue square: contrast after DBC addition. (D) Topographic image of the EPC bilayer at the region marked by the blue square. (E) Phase image of DMPC bilayer. Blue square: region of the EPC bilayer surface where a small area topographic image (F) was acquired. (G) Phase image of the same structures in (E) after DBC addition. Blue square: contrast after DBC addition. (H) Topographic image of the DMPC bilayer at the region marked by the blue square. The topographies shown at (B) and (F) basically show noise levels in the images. (For interpretation of the references to colour in this figure legend, the reader is referred to the web version of this article.)

(lipid–water) hydrogen bonds. Thus, the structures observed in Fig. 7 could be interpreted as dibucaine aggregates bound to the bilayer surface. However, our experiments were made below the dibucaine CMC range reported in literature (30–140 mM) [37,43]. In order to have a more quantitative analysis of the height and radius of the "budding" structures, we have determined the number, radius and height of particles associated to them using commercially available softwares.[2] For DMPC these measurements show that the height increases (from 0.1 to 0.3 nm) with the incubation time while the radius is kept approximately constant (~34 nm) as shown in Fig. 8. Moreover, the shape of the structures does not characterize the formation of different lipid domains on the surface, since the height variation is smooth, with no clear edges or boundaries defining these structures. Considering that this effect is due to DBC interaction with the PC polar head group, we can argue that DBC is not homogeneously distributed along the bilayer surface; its concentration in the surface could, however, build up in time leading to the increasing number of surface structures and associated variation in the phase image. Indeed, the number of surface structures increases from 10 to 70 in each $1.5 \times 1.5\ \mu m^2$ area as time proceeds along the experiment. The increase in height of these structures occurs usually prior to the membrane rupture, indicating that local stresses may have reached a maximum value.

Changes in morphology of model membranes due to their interaction with anesthetic molecules have been reported in literature. Leonenko et al. [12] studied the effects of the general anesthetic halothane on PC bilayers. They observed the appearance of new thinner domains (with 3.5 nm in height) in an initially uniform bilayer (5.5 nm in height), after incorporation of the anesthetic. Thus AFM images in that work show patches with a height difference of 2 nm. However, halothane is a neutral and general anesthetic with action in the Central Nervous System while DBC is a protonated (at the experimental condition) local anesthetic which acts on the voltage-dependent sodium channels on excitable membranes. In our case, changes in the bilayer surface morphology are much smaller; moreover, the height and radius dependence on DBC concentration or incubation time, shown in Fig. 8, suggests changes of the local curvature of the bilayer induced by DBC. Despite phospholipid molecules present a critical packing parameter [44] coherent with planar structures, we can not reject the possibility that in the presence of a certain DBC amount, changes in the critical curvature radius may occur. The change in the membrane curvature has been considered as a possible mechanism for local anesthetic action in membranes. Baciu et al [45] observed that protonated local anesthetics (Lidocaine, Prilocaine) and Ketamine induced increasing

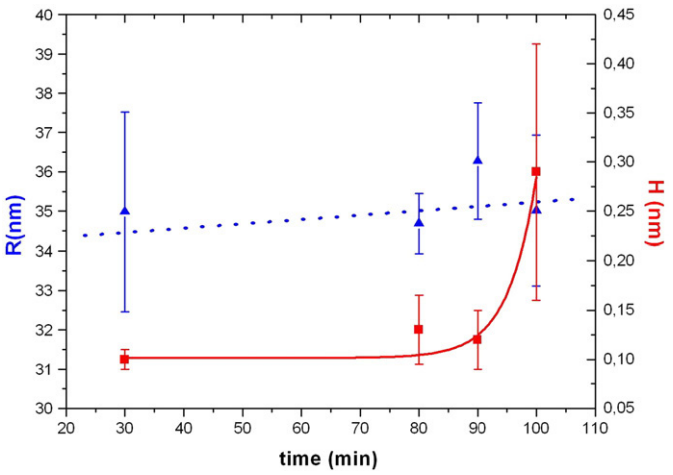


**Fig. 8.** Measurements for height and radius for the small 'structures' formed on the DMPC bilayer surface as a function of time after DBC addition (final concentration in liquid cell: 5 mM).

[2] The values in Fig. 8 represent the average values for the particles found at each topographic image along the time of the experiment.

curvature of the membrane after penetrating its surface. The authors also reported the formation of pores associated to the incorporation of the drug. These results altogether lead us to propose that DBC induces local curvature changes followed by the disruption of the lipid bilayers. These assumptions were further investigated through adsorption kinetics and elasticity measurements as reported in the next section.

### 3.3. DBC adsorption at lipid monolayers

The lipids used in this study have the same polar zwitterionic head group, phosphatidylcholine, however they differ in the apolar portion of the molecule. DMPC holds a completely saturated double chain with 14 carbons, while EPC is a mixture of many natural lipids extracted from hen egg yolk, containing different chain length and unsaturated molecules, mostly 16:0 (*sn1*) and 18:1 or 18:2 (*sn2*) apolar chains. Consequently they present different behaviors at the air/liquid interface as shown by their $\pi$–*A* curves in Fig. 9. EPC monolayers display, at 24 °C, an incipient phase transition around 30 mN m$^{-1}$. Both DMPC and EPC monolayers exhibit $\pi$–*A* isotherms presenting an expanded characteristic with minor differences in the surface compressional modulus values, $Cs^{-1}=-(d\pi/d\ \ln A)$. At 30 mN m$^{-1}$ and 24 °C, $Cs^{-1}$ are about 73.5 mN m$^{-1}$ and 88 mN m$^{-1}$, respectively for EPC and DMPC monolayers. Whereas the $Cs^{-1}$ value for DMPC agrees with those in the literature [46], measured in a temperature lower than that used in the present study, the value for EPC is lower, much likely due the phase transition of DMPC, observed at 24 °C. Therefore DMPC is slightly more condensed than EPC monolayers, as expected by the saturated structure of the former phospholipid.

Fig. 10 shows the adsorption kinetics at 2.72 mM DBC for EPC and DMPC monolayers. As presented in the previous section, at this DBC concentration changes in the surface morphology begin to be detectable from the AFM images, in the case of EPC. Previous report [47] showed that the adsorption kinetics of a protein in a lipid monolayer by the pendant drop technique can be related with both injection and subphase formation methods in a Langmuir through. The first methodology consists in the injection of the soluble molecule in the subphase of a preformed lipid monolayer. This method is quite equivalent to the AFM measurements. The second one is the spreading of the lipid monolayer on the surface of the molecule solution. Comparing the methodologies, the authors concluded that adsorption of protein molecules on the new monolayer, from the subphase, is similar to the adsorption by the injection method, and it takes the advantage of the bulk homogeneity [47]. In addition, for both

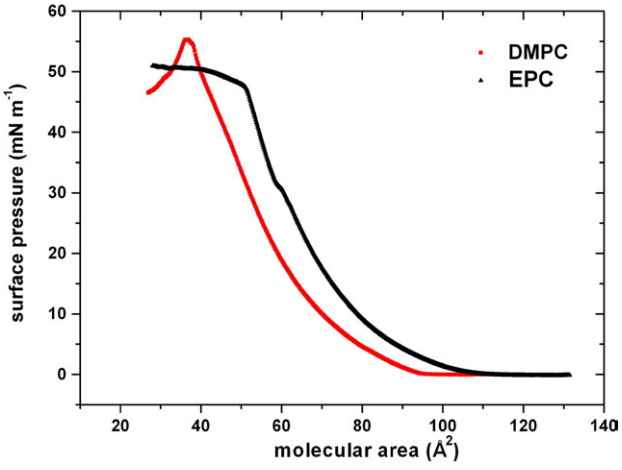


**Fig. 9.** Surface Pressure isotherms for (black) EPC and (red) DMPC monolayers. (For interpretation of the references to colour in this figure legend, the reader is referred to the web version of this article.)

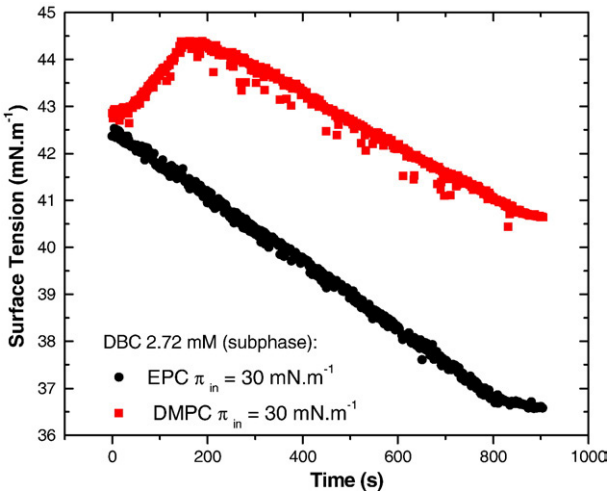


**Fig. 10.** Adsorption kinetics for DBC on EPC (black curve) and DMPC (red curve) monolayers, both at an initial surface pressure of 30 mN m$^{-1}$. (For interpretation of the references to colour in this figure legend, the reader is referred to the web version of this article.)

experiments performed in our work, membrane prepared from vesicles for AFM analysis and phospholipid monolayer in the adsorption kinetics experiments, the hydrophilic head groups can be accessed by DBC which binds to the polar head group of phospholipids [35–38].

Surface tension curves for EPC and DMPC show slightly different behaviors. For EPC the curve presents a simple decay, indicating a one step adsorption. For DMPC, however, an induction time, with an initial increase in the surface tension values, is observed, followed by a continuous decrease, until the system reaches the equilibrium. However, it is worthwhile to stress that both phospholipid monolayers were kept initially at 30 mN m$^{-1}$ (correspondent to a surface tension of 42.8 mN m$^{-1}$) and, in this sense, the interaction of dibucaine with EPC is instantaneous (considering the time resolution of our experiments of 200 ms) since the decreasing in surface tension is recorded from the very first measured point. The equilibrium of adsorption, however, is reached only after ca. 15 min. The differences in surface phases (DMPC more condensed than EPC) for these two monolayers at 30 mN m$^{-1}$ should be the reason for the quite different profile observed for the adsorption kinetics of these two lipids. We could suggest that for the more expanded EPC monolayers, the penetration of dibucaine molecules is easier; the larger probability of bidimensional deformation of the monolayer could be due to the loose surface packing. On other hand, for DMPC, which produces more condensed monolayers, the observed induction time is probably related to the electrostatic interaction of dibucaine molecules with the polar head groups [48] of the phospholipid in an initial step, with no significant changes in the orientation of the phospholipid molecules, since they already present a tight packing. After that, the anesthetic is able to adsorb at the interface, by inserting within the phospholipid molecules, causing a decrease in the surface tension until the system reaches the equilibrium.

### 3.4. Dilatational surface elasticity measurements

The effect of dibucaine on DMPC and EPC monolayers could also be investigated by dilatational surface elasticity. For an insoluble one-component system this kind of technique can give information on how easily the system recovers a surface tension value, after a perturbation in area variation. The higher the dilatational elasticity modulus, E, the more difficult is the change in the surface packing by compression-expansion sequences. The E values for DMPC and EPC at 30 mN m$^{-1}$ are 110 mN m$^{-1}$ and 87 mN m$^{-1}$, respectively, in

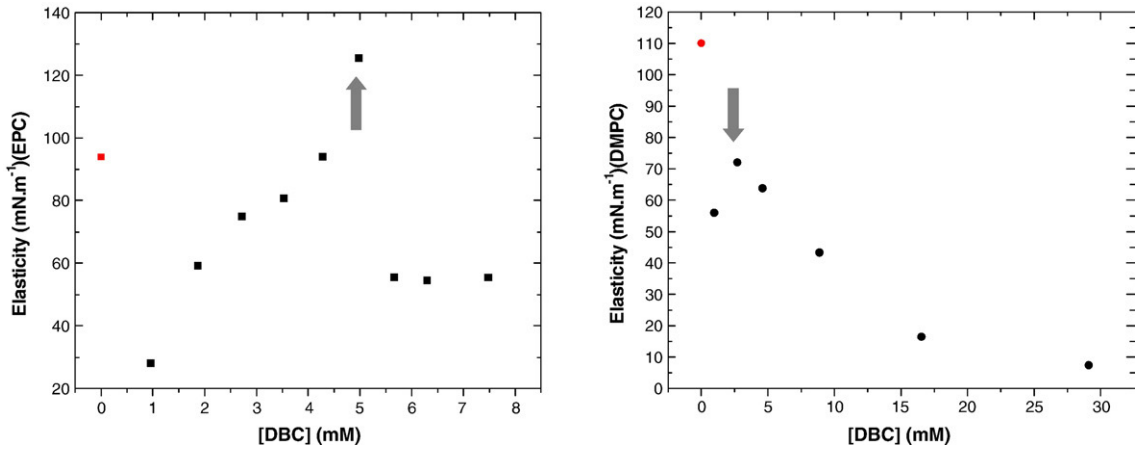


**Fig. 11.** Effect of dibucaine on dynamic dilatational surface elasticity modulus (E) of DMPC (right) and EPC (left) monolayers, as measured at 30 mN $m^{-1}$ by the pendant drop technique using the axissymmetric drop shape analysis method. Arrows: concentrations where the maximum appears coincide with those for which a disruption of the bilayer was observed in AFM experiments. Red point: ***E*** value for pure phospholipid in the absence of DBC. (For interpretation of the references to colour in this figure legend, the reader is referred to the web version of this article.)

accordance with their equilibrium compressional moduli already presented before. In Fig. 11 (A) and (B) one can see the effect of dibucaine on E for both phospholipids. In common there is the presence of a maximum in a given dibucaine concentration, which is dependent on the kind of phospholipid — around 2.7 mM for DMPC and 5.0 mM for EPC. From AFM experiments the concentrations where the maximum appears are close to the values for which a disruption of the bilayer was observed (arrows, Fig. 11).

Studies of DMPC mono and bilayers [49] have shown that their surface elasticities decrease in the presence of alkanol series which are also known to act as an anesthetic and penetration enhancer. However in that study the authors only compared the equilibrium value of elasticity (or better, its inverse, the isothermal compressibility) at the onset of the liquid expanded phase and for a constant tetradecanol concentration. In the present work we could attest that there is a dependence with the DBC concentration for this effect. The same general trend is obtained for both phospholipids, that is, a significant decrease of elasticity in the presence of small amounts of the anesthetic, as compared with the elasticities for the pure phospholipid monolayers, followed by a maximum with subsequent increasing of DBC concentration.

We suggest that, at low concentrations, DBC is incorporated into the interface, mainly affecting the ordering of the monolayer. However, the new mixed monolayer formed in this way may become more packed with the addition of DBC, until a certain critical DBC:lipid molar ratio is reached, for which the monolayer can even be disrupted. From this point E exhibits a steep decrease indicating that the monolayer can no longer be regenerated. Despite the similar behavior observed for both lipids, the concentration range and the relative decrease in E, compared to the values observed for the respective pure monolayers are different. For the DMPC monolayer, the maximum is observed at lower DBC concentration and smaller relative E value compared to the pure monolayer. It is also important to notice that for DBC in EPC the maximum E value surpass the one obtained for pure EPC monolayers, indicating that in a small range of concentrations, DBC may help to restore the equilibrium surface tension condition or surface packing of the EPC monolayer.

The decrease in E values after the maximum can indicate a local disruption of the monolayer. From AFM experiments we observed that the disruption effect occurs first where a large perimeter/area ratio favors the DBC insertion — for example at the edges of the DMPC patches and the EPC aggregates. This effect, as well as the height variations along the bilayer surface in the topography images, was observed for DBC concentrations above the maximum E value. A similar effect has been reported by Moradat and Kirat [50] who observed bilayer disruption under detergent action. Those authors attributed this effect to the formation of lipid-detergent mixed micelles in the solution. Nomura et al [51] reported a decrease in EPC liposome sizes in the presence of the same detergent, as an indication of the mixed micelles formation. In fact mixed micelles containing phospholipids were also observed in the presence of cholesterol [52], sodium taurocholate [53] and other lipids [54]. From our results the disruption of the monolayer under dilatational stress above a certain amount of dibucaine may represent a driving force for DBC-lipid mixed micelles formation. Therefore, this mechanism could also be a likely explanation for the observed disruption in AFM images.

This assumption can be understood based on our AFM and elasticity measurements. According to the latter, the lipid monolayer becomes more packed with the continuous addition of DBC thus providing a maximum in elasticity. If we correlate these results to the bilayer observations with the AFM, we may assume that the initially small height variations (~0.1 nm) in the topography images represent a first-stage DBC insertion mechanism in the bilayer, closer to the PC polar head. Since our bilayer images present some roughness (~0.2 nm), we can not detect the height variation except in regions where larger molecule concentrations can be found, leading to a low spatial frequency roughness in the topography images. At a second stage, a deeper DBC insertion in the bilayer – at least for DMPC – leads to larger local stresses, increasing the local curvature in the process, which may eventually induce the formation of DBC-lipid mixed micelles. Once the stress can no longer be accommodated by the bilayer, rupture occurs. This scenario can also be expected to occur at a faster rate in regions where DBC insertion is facilitated, like the patch edges. The presence of a mixed material prior to the rupture agrees with the observed variations in the AFM phase images.

## 4. Conclusions

In summary, our results suggest a modification of the molecular packing of EPC and DMPC bilayer or monolayer surfaces due to the DBC interaction with the polar head group of the lipids. A progressive disruption of these layers is observed with increasing incubation times and DBC concentration, probably due to mixed micelle formation. Dilatational elasticity measurements show that this property is strongly affected by the presence of DBC in the drop's subphase solution, for both lipids. Changes in local curvature, as observed in our samples, can be responsible for different structural characteristics of the membranes studied, thus giving support to transport models

where the lipid phase is indeed relevant to the biophysical properties of biological membranes.

## Acknowledgments

The authors wish to thank Dr. Tânia Creczynski Pasa for useful discussions and Marcio A. Paschoal for technical assistance. This work was financially supported by FAPESP and CNPq. The authors (G.S.L., T. M. N.) acknowledge scholarships from CAPES and CNPq. M.E.D.Z, E.P. and M.A.C. are CNPq research fellows.

## Appendix A. Supplementary data

Supplementary data associated with this article can be found, in the online version, at doi:10.1016/j.bpc.2008.10.006.

## References

[1] C. Bieri, O.P. Ernst, S. Heyse, K.P. Hofmann, H. Vogel, Micropatterned immobilization of a G protein-coupled receptor and direct detection of G protein activation, Nat. Biotechnol. 17 (1999) 1105–1108.
[2] I. Reviakine, W. Bergsma-Schutter, A. Brisson, Growth of protein 2-d crystals on supported planar lipid bilayers imaged in situ by AFM, J. Struct. Biol. 121 (1998) 356–362.
[3] E. Sackmann, Supported membranes: scientific and practical applications, Science 271 (1996) 43–48.
[4] A.T.A. Jenkins, J. Hu, Y.Z. Wang, S. Schiller, R. Foerch, W. Knoll, Pulsed plasma deposited maleic anhydride thin films as supports for lipid bilayers, Langmuir 16 (2000) 6381–6384.
[5] L. Kam, S.G. Boxer, Spatially selective manipulation of supported lipid bilayers by laminar flow: Steps toward biomembrane microfluidics, Langmuir 19 (2003) 1624–1631.
[6] C. Larsson, M. Rodahl, F. Hook, Characterization of DNA immobilization and subsequent hybridization on a 2D arrangement of streptavidin on a biotin-modified lipid bilayer supported on $SiO_2$, Anal. Chem. 75 (2003) 5080–5087.
[7] H.M. McConnell, T.H. Watts, R.M. Weis, A.A. Brian, Supported planar membranes in studies of cell–cell recognition in the immune system, Biochim. Biophys. Acta 864 (1986) 95–106.
[8] N.L. Thompson, A.F. Palmer, Model cell membranes on planar substrates, Comments Mol. Cell. Biophys. 5 (1988) 39–56.
[9] J.K. Seydel, M. Wiese (Eds.), Drug–membrane interaction, Wiley-VCH, Weinheim, 2002.
[10] J.K. Seydel, E.A. Coats, H.P. Cordes, M. Wiese, Drug membrane interaction and the importance for drug transport, distribution, accumulation, efficacy and resistance, Arch. Pharm. 327 (1994) 601–610.
[11] A. Berquand, MM.P. Mingeot-Leclercq, Y.F. Dufrêne, Real-time imaging of drug-membrane interactions by atomic force microscopy, Biochim. Biophys. Acta 1664 (2004) 198–205.
[12] Z. Leonenko, E. Finot, D. Cramb, AFM study of interaction forces in supported plana DPPC bilayers in the presence of general anesthetic halothane, Biochim. Biophys. Acta 1758 (2006) 487–492.
[13] B.G. Covino, H.G. Vassallo, Local Anesthetics: Mechanisms of Action and Clinical Use, Grune and Stratton, New York, 1976.
[14] G.R. Strichartz, J.M. Ritchie, Local anesthetics, in: G.R. Strichartz (Ed.), Handbook of Experimental Pharmacology, vol. 81, Springer-Verlag, Berlin, 1987, chap. 2.
[15] J.F. Butterworth, G.R. Strichartz, Molecular mechanisms of local anesthesia: a review, Anesthesiology 72 (1990) 711–734.
[16] F. Yanagidate, G.R. Strichartz, Local anesthetics, Handb. Exp. Pharmacol. 177 (2006) 91–123.
[17] E. de Paula, S. Schreier, Molecular and physicochemical aspects of local anesthetic-membrane interaction, Braz. J. Med. Biol. Res. 9 (1996) 877–894.
[18] E. de Paula, H.C. Jarrell, S. Schreier, L.F. Fraceto, Preferential location of lidocaine and etidocaine in lecithin bilayers as determined by EPR, fluorescence and 2H-NMR, Biophys. Chem. 132 (2008) 47–54.
[19] Z.F. Shao, Y.Y. Zhang, Biological cryo atomic force microscopy: a brief review, Ultramicroscopy 66 (1996) 141–152.
[20] R.C. Advincula, W. Knoll, L. Blinov, C.W. Frank, Langmuir and Langmuir–Blodgett–Kuhn films of poly(vinylidene fluoride) and poly(vinylidene fluoride-co-trifluoroethylene) alternated with poly(methyl methacrylate) or poly(octadecyl methacrylate), Org.Thin Films 695 (1998) 192–205.
[21] M. Edidin, The state of lipid rafts: from model membranes to cells, Annu. Rev. Biophys. Biomol. Struct. 32 (2003) 257–283.
[22] K. Kamata, S. Manno, M. Ozaki, Y. Takakuwa, Functional evidence for presence of lipid rafts in erythrocyte membranes: Gsa in rafts is essential for signal transduction, Am. J. Hematol. (2008) 1–5.
[23] H. Mueller, H.J. Butt, E. Bamberg, Imaging the myelin basic protein adsorbed to lipid bilayers with the atomic force microscopy, J. Phys. Chem. B 104 (2000) 4552–4559.
[24] P.E. Milhiet, M.C. Giocondi, O. Baghdadi, F. Ronzon, C. Le Grimellec, B. Roux, AFM detection of GPI protein insertion into DOPC/DPPC model membranes, Single Mol. 2–3 (2002) 136–141.
[25] L. Caseli, T.M. Nobre, D.A.K. Silva, W. Loh, M.E.D. Zaniquelli, Flexibility of the triblock copolymers modulation their penetration and expulsion mechanism in Langmuir monolayers of dihexadecyl phosphoric acid, Colloids Surf. B, Biointerfaces 22 (2001) 309–321.
[26] F.J. Pavinatto, A. Pavinatto, L. Caseli, D.S. dos Santos, T.M. Nobre, M.E.D. Zaniquelli, O.N. Oliveira, Interaction of chitosan with cell membrane models at the air–water interface, Biomacromolecules 8 (2007) 1633–1640.
[27] T.M. Nobre, K. Wong, M.E.D. Zaniquelli, Equilibrium and dynamic aspects of dodecytrimethylammonium bromide adsorption at the air/water interface in the presence of λ-carrageenan, J. Colloid Interface Sci. 305 (2007) 142–149.
[28] Z.V. Leonenko, A. Carnini, D.T. Cramb, Supported planar bilayer formation by vesicle fusion: the interaction of phospholipid vesicles with surfaces and the effect of gramicidin on bilayer properties using atomic force microscopy, Biochim. Biophys. Acta 1509 (2000) 131–147.
[29] H. Egawa, K. Furusawa, Liposome Adhesion on Mica Surface Studied by Atomic Force Microscopy, Langmuir 15 (1999) 1660–1666.
[30] D. Marsh, Lateral pressure in membranes, Biochim. Biophys. Acta 1286 (1996) 183–223.
[31] V.B. Fainerman, D. Möbius, R. Miller, Surfactants: Chemistry, Interfacial Properties, Applications, Elsevier, The Netherlands, 2001.
[32] J. Lucassen, M. van den Tempel, Dynamic measurements of dilational properties of a liquid interface, Chem. Eng. Sci. 27 (1972) 1283.
[33] C. Yuan, L.J. Johnston, Atomic force microscopy studies of ganglioside GM1 domains in phosphatidylcholine and phosphatidylcholine/cholesterol bilayers, Biophys. J. 81 (2001) 1059–1069.
[34] I. Reviakine, A. Brisson, Formation of supported phospholipid bilayers from unilamellar vesicles investigated by atomic force microscopy, Langmuir 16 (2000) 1806–1815.
[35] P.R. Cullis, A.J. Verkleij, Modulation of membrane-structure by $Ca^{2+}$ and dibucaine as detected by P-31 NMR, Biochim. Biophys. Acta 552 (1979) 546–551.
[36] M.R. Eftink, R.K. Puri, M.D. Ghahramani, Local anesthetic phospholipid interactions — the pH-dependence of the binding of dibucaine to dimyristoylphosphatidylcholine vesicles, Biochim. Biophys. Acta 813 (1985) 137–140.
[37] M. Wakita, Y. Kuroda, Y. Fujiwara, T. Nakagawa, Conformations of dibucaine and tetracaine in small unilamellar phosphatidylcholine vesicles as studied by nuclear Overhauser effects in 1H nuclear magnetic resonance spectroscopy, Chem. Phys. Lipids 62 (1992) 45–54.
[38] I. Ueda, J.-S. Chiou, P.R. Krishna, H. Kamaya, Local anesthetics destabilize lipid membranes by breaking hydration shell: Infrared and calorimetry studies, Biochim. Biophys. Acta 1190 (1994) 421–429.
[39] F. Tokumaso, A.J. Jin, J.A. Dvorak, Lipid membrane phase behavior elucidated in real time by controlled environment atomic force microscopy, J. Electron Microsc. 51 (2002) 1–9.
[40] A.F. Xie, R. Yamada, A.A. Gewirth, S. Granick, Materials science of the gel to fluid phase transition in a supported phospholipid bilayer, Phys. Rev. Lett. 89 (2002) 243103–1–243103-4.
[41] S.V.P. Malheiros, L.M.A. Pinto, L. Gottardo, D.K. Yokaichiya, L.F. Fraceto, N.C. Meirelles, E. de Paula, A new look at the hemolytic effect of local anesthetics, considering their real membrane/water partitioning at pH 7.4, Biophys. Chem. 110 (2004) 213–221.
[42] S. Kaneshina, H. Satake, T. Yamamoto, Y. Kume, H. Matsuki, Partitioning of local anesthetic dibucaine into bilayer membranes of dimyristoylphosphatidylcholine, Colloids Surf. B, Biointerfaces 10 (1997) 51–57.
[43] H. Matsuki, M. Yamanaka, S. Kaneshina, H. Kamaya, I. Ueda, Surface tension study on the molecular-aggregate formation of local anesthetic dibucaine hydrochloride, Colloids Surf. B, Biointerfaces 11 (1998) 87–94.
[44] J.N. Israelachvilli, J.D. Mitchell, B.W. Ninham, Theory of self-assembly of hydrocarbon amphiphiles into micelles and bilayers, J. Chem. Soc., Faraday Trans. 272 (1976) 1525–1568.
[45] M. Baciu, M.C. Holmes, M.S. Leaver, morphological transitions in model membrane systems by addition of anesthetics, J. Phys. Chem. B 111 (2007) 909–917.
[46] N. Vernoux, O.M.F. Besson, T. Granjon, O. Marcillat, C. Vial, Mitochondrial creatine kinase adsorption to biomimetic membranes: a Langmuir monolayer study, J. Colloid Interface Sci. 310 (2007) 436–445.
[47] T.F. Schmidt, L. Caseli, T.M. Nobre, M.E.D. Zaniquelli, O.N. Oliveira Jr., Interaction of horseradish peroxidase with Langmuir monolayers of phospholipids, Colloids Surf. A, Physicochem. Eng. Asp. 321 (2008) 206–210.
[48] G. Schwarz, L. Damian, M. Winterhalter, Model-free analysis of binding at lipid membranes employing micro-calorimetric measurements, Eur. Biophys. J. 36 (2007) 571–579.
[49] B. Griepernau, S. Leis, M.F. Schneider, M. Sikor, D. Steppich, R.A. Böckmann, 1–Alkanols and membranes: a story of attraction, Biochim. Biophys. Acta — Biomembranes 1768 (2007) 2899–2913.
[50] S. Morandat, K.E. Kirat, Membrane resistance to Triton X-100 explored by real time atomic force microscopy, Langmuir 22 (2006) 5786–5791.
[51] F. Nomura, M. Nagata, T. Inaba, H. Hiramatsu, H. Hotani, K. Takiguchi, Capabilities of liposomes for topological transformation, Proc. Natl. Acad. Sci. 98 (2001) 2340–2345.
[52] D. Juengst, T. Lang, P. Huber, V. Lange, G. Paumgartner, Effect of phospholipids and bile acids on cholesterol nucleation time and vesicular/micellar cholesterol in gallbladder bile of patients with cholesterol stones, J. Lipid Res. 34 (9) (1993) 1457–1464.
[53] F.J. Castellino, B.N. Violand, Phosphorus-31 nuclear magnetic resonance and 31P{1H} nuclear Overhauser effect analysis of mixed egg phosphatidylcholine-sodium taurocholate vesicles and micelles, Arch. Biochem. Biophys. 193 (2) (1979) 543–550.
[54] G. Lipka, H. Hauser, Phase behavior of mixtures of lipid X with phosphatidylcholine and phosphatidylethanolamine, Biochim. Biophys. Acta 979 (1989) 239–250.